Investigation of the AVR Output Voltage Limits in Power System Voltage Stability Assessment

Hadi Razmi

***Abstract*— Voltage stability problems have been one of the major concerns for electric power utilities due to increased interconnections and loading of the present day power systems. The accurate representation of the voltage instability phenomena requires a detailed model of power system components (generators, transformers, loads, etc.). On the other hand, reactive power generation limits have a significant effect on voltage collapse. In general, the system equations change non-smoothly when these limits are encountered.**

This paper presents a continuation-based method to steady-state voltage stability analysis that considered complete model of power system and the automatic voltage regulator (AVR) output voltage limits that indirectly control the reactive power generation limits. Results are provided for the New England 39-bus power system model. By comparing results obtained through this method and the continuation power flow (CPF) method, it is concluded that for design and developing the power systems, using proposed method seems a better approach due to its higher accuracy.

***Index Terms*— steady-state voltage stability, automatic voltage regulator (AVR) output voltage limit, power system differential-algebraic equation (DAE) model.**

I. INTRODUCTION

Increasing energy demand along with shortages in installed production capacities have resulted in operating power systems at their security boundaries. Generally, these boundaries are defined by thermal and transient stability. With recent achievements in designing quick excitation systems, synchronized phasor measurements and stability control devices, transient stability problems have been reduced significantly [1]. However, by growing large power systems, a new phenomenon has been observed, which is referred to as voltage instability or voltage collapse [2, 3]. Voltage stability is concerned with the ability of a power system to maintain acceptable voltages at all buses of the system under normal conditions and after occurrence of a disturbance. A system enters a state of voltage instability when a disturbance, increase in load demand, or change in system conditions causes a progressive and uncontrollable decline in voltage and the process may result in voltage collapse.

Traditional methods of static voltage stability analysis, like P-V curve, Q-V curve, minimum eigenvalue, right eigenvector, reduced Jacobian, sensitivity analysis and energy based methods rely on the power flow model [4]. These methods have difficulty in evaluating voltage stability due to using simple models for system components such as generators. To improve voltage stability analysis, a detailed dynamic representation of the power system is required.

Manuscript Received on May, 2014.

Dr. Hadi Razmi, Department of Engineering, East Tehran Branch, Islamic Azad University, Tehran, Iran.

Furthermore, it is very important to reasonably represent the system limits when voltage stability is being studied. Therefore, the reactive power limit of generators is known to greatly affect the voltage stability [5, 6]. If the reactive power reaches its upper limit as the result of a gradual increase in the load demand, the system stability may change discontinuously. In the worst case, a stable system may suddenly become unstable. This case is referred to as a Saddle Limit Induced Bifurcation (SLIB).

In this paper, a new methodology based on the predictor-corrector method is introduced for the steady state voltage stability assessment of power systems. This methodology simultaneously traces the total system equilibrium of the limited power system model while the total system Jacobian matrix remains unchanged during continuation. The paper is organized as follows:

In section II, a detailed model of the power system components are described. The continuation based method for the steady state voltage stability assessment is presented in section III. Section IV presents the numerical results obtained by the steady state voltage stability assessment of the New England 39-bus power system model in various operating conditions. Finally, section V concludes the paper.

II. POWER SYSTEM MODEL

- A power system is assumed to have *n* busses and *m* generators.
- A two-axis synchronous machine model is used which consists of four differential equations as described in [7, 8].
- The simplified IEEE type DC-1 excitation system is used here. The corresponding mathematical model is found in [7, 8].
- A simplified prime mover and speed governor is used here. Two differential equations for the description of its dynamics are expressed in [7].
- The remaining elements of the power system are represented by their static models or power flow models. It is noted that the voltage collapse phenomenon is a relatively slow process; thus, the effect of fast dynamics or short period phenomena can be ignored [9].
- Controllers that result in a variable structure system, such as unified power flow controller (UPFC), are not considered in the model.
- Only off load tap changing is taken into consideration.
- Only the PQ constant load model has been used to represent the demand busses.

Corresponding to the above models and assumptions, the network equations can be written as [7]. In voltage stability studies, differential and algebraic equations should be generalized.

To establish a generalized form of equations, λ is introduced as a parameter representing load variations [10].
The power system differential and algebraic equations (DAEs) can be simply represented by Eqs. (1) and (2).

$$\dot{\bar{X}} = \bar{F}(\bar{X}, \bar{Y}, \bar{P}) \quad (1)$$

$$\bar{0} = \bar{G}(\bar{X}, \bar{Y}, \bar{P}) \quad (2)$$

The state vector $\bar{X}$ and algebraic vector $\bar{Y}$ contain the following variables;

$$\bar{X} = (\bar{\delta}, \bar{\omega}, \bar{E}'_q, \bar{E}'_d, \bar{P}_m, \bar{\mu}, \bar{E}_{fd}, \bar{V}_r, \bar{R}_f) \quad (3)$$

$$\bar{Y} = (\bar{V}, \bar{\theta}) \quad (4)$$

Where:

- δ_i is the i^{th} generator's rotor angle.
- ω_i is the i^{th} machine frequency, namely, the i^{th} generator angular speed;
- E'_{d_i} and E'_{q_i} are transient direct axis and quadrature axis EMF of the i^{th} machine, respectively;
- P_{m_i} is the i^{th} mechanical power of the prime mover;
- μ_i is the i^{th} steam valve or water gate opening;
- E_{fd_i} is the voltage applied to the i^{th} generator field winding;
- V_{r_i} and R_{f_i} are the outputs of the i^{th} AVR and exciter soft feedback, respectively;

The $\bar{P}$ in Eqs. (1) and (2) can be further divided into control vector $\bar{U}$ and parameter vector $\bar{Z}$.

$$\bar{U} = (\bar{V}_{ref}, \bar{P}_{Gd_0}, \cdots), \quad \bar{Z} = (\bar{P}_L, \bar{Q}_L) \quad (5)$$

Where, V_{ref_i} is the reference voltage of the i^{th} AVR. In short, $\bar{X}$ contains all the system state variables; $\bar{Y}$ includes the algebraic variables; $\bar{U}$ is the control vector, while $\bar{Z}$ characterizes the system loading condition.
A system of an equilibrium solution is needed for evaluating the stability analysis. The solutions of Eqs. (1) and (2) at the steady state condition, when $\dot{\bar{X}} = \bar{0}$, yields to the equilibrium points. By setting the differential equations to zero, a state of equilibrium of the system will be obtained.
Once the i^{th} AVR saturates, it loses the ability to adjust V_{r_i}, and consequently the reactive power Q_{G_i} to meet the load demand. By referring to Eqs. (1) and (2), the dynamic differential equations at the steady state condition will be dropped and will not be included for the stability analysis. In other words, the saturated dynamic state would be considered as a steady state variable and therefore, it will stay as a constant in the DAEs. Hence, it no longer participates in the dynamic response of the power system. If we solve the DAEs, we may not be able to find a solution. This is because, when the loads increase further, in order to continuously keep V_{r_i} at the maximum value, V_{ref_i} should be reduced. The decrease of V_{ref_i}, reflects the inability of the generator to keep pace with the load increase.

III. STEADY STATE POWER SYSTEM ANALYSIS

Similar approach to CPF can be applied to trace the total equilibrium as defined by Eqs. (1) and (2) at the steady state condition. To start power system equilibrium tracing, we need initial conditions that are defined by the state variables (i.e. $\bar{\delta}, \bar{\omega}, \bar{E}'_q, \bar{E}'_d, \bar{P}_m, \bar{\mu}, \bar{E}_{fd}, \bar{V}_r, \bar{R}_f$) at the generation busses and the algebraic variables of $\bar{V}, \bar{\theta}$ at all busses. The solution from the power flow method provides $\bar{V}$ and $\bar{\theta}$ at all busses. The remaining values obtained are described in [7].
The system equilibrium manifold defined by Eqs. (1) and (2) at the steady state condition could be traced, according to a scheduled scenario parameterized by λ. The tracing is going to be obtained through the generation of continuous solutions from the base case (initial conditions) at $\lambda = 0$ up to the critical point at $\lambda = \lambda^{critical}$ where voltage collapse associated with the SNB (Saddle Node Bifurcation) or SLIB occurs. A locally parameterized continuation (LPC) technique was proposed by Rheinbolds [11]. In order to evaluate the stability margin, the system equilibrium tracing utilizes LPC to solve Eqs. (1) and (2) at the steady state condition.

A. Predictive stage

At this stage, an approximate solution is derived starting from the base case and in the direction of the tangent vector. Therefore, the first task is to calculate the tangential vector, which can be derived by differentiating both sides of Eqs. (1) and (2) at the steady state condition.

$$d\bar{F} = \bar{F}_{\bar{X}} d\bar{X} + \bar{F}_{\bar{Y}} d\bar{Y} + \bar{F}_{\lambda} d\lambda \quad (6)$$

$$d\bar{G} = \bar{G}_{\bar{X}} d\bar{X} + \bar{G}_{\bar{Y}} d\bar{Y} + \bar{G}_{\lambda} d\lambda \quad (7)$$

It yields:

$$\begin{bmatrix} d\bar{F} \\ d\bar{G} \end{bmatrix} = J.\bar{t}; \ with \ J = \begin{bmatrix} \bar{F}_{\bar{X}} & \bar{F}_{\bar{Y}} & \bar{F}_{\lambda} \\ \bar{G}_{\bar{X}} & \bar{G}_{\bar{Y}} & \bar{G}_{\lambda} \end{bmatrix} \quad (8)$$

$$and \ \bar{t} = [d\bar{X} \quad d\bar{Y} \quad d\lambda]^T$$

Where, J is a $(2n+10m)\times(2n+10m+1)$ matrix and $\bar{t}$ is a $(2n+10m+1)\times 1$ vector. The tangential vector $\bar{t}$ yields to;

$$J.\bar{t} = \bar{0} \quad (9)$$

On the left side of this equation, a matrix of partial derivatives is multiplied by a vector of differentials. The former is the total system Jacobian matrix augmented by one column ($[\bar{F}_{\lambda} \quad \bar{G}_{\lambda}]^T$), while the latter is the tangent vector being sought. There is, however, an important barrier to overcome before a unique solution can be found for the tangent vector. The problem arises from the fact that one additional unknown parameter was added when λ was inserted into the power system equations, but the number of equations remained unchanged. Thus, one more equation is needed. This problem can be solved by choosing a non-zero magnitude (say one) for one of the components of the tangent vector, i.e. $\bar{e}_k^T \bar{t} = a_k$. This results in;

$$\begin{bmatrix} \bar{F}_{\bar{X}} & \bar{F}_{\bar{Y}} & \bar{F}_{\lambda} \\ \bar{G}_{\bar{X}} & \bar{G}_{\bar{Y}} & \bar{G}_{\lambda} \\ & \bar{e}_k^T & \end{bmatrix} \bar{t} = \begin{bmatrix} \bar{0} \\ \bar{0} \\ a_k \end{bmatrix} \quad (10)$$

Where, $\bar{e}_k^T$ is an appropriately dimensioned row vector with all its elements equal to zero except the k^{th} element, which is equal to one. If the index k is chosen correctly, letting $a_k = \pm 1$, a non-zero norm on the tangent vector is imposed and guarantees that the augmented Jacobian matrix will be nonsingular at the critical point, where $\bar{F}_{\bar{X}}$ and $\bar{G}_{\bar{X}}$ cannot be null vectors at the same time even at the base case ($\lambda = 0$) [12]. Depending on how the k^{th} state variable is changing, the values +1 or -1 may be selected. For increasing and decreasing, +1 and -1 are chosen, respectively. Once the tangent vector has been found by solving Eq. (10), the prediction is made as follows;

$$\begin{bmatrix} \bar{X}^* \\ \bar{Y}^* \\ \lambda^* \end{bmatrix} = \begin{bmatrix} \bar{X} \\ \bar{Y} \\ \lambda \end{bmatrix} + \sigma \begin{bmatrix} d\bar{X} \\ d\bar{Y} \\ d\lambda \end{bmatrix} \quad (11)$$

Where, '*' denotes the predicted solution for a subsequent value of λ (loading) and σ is a scalar that designates the step size. The step size should be chosen so that the predicted solution is within the radius of convergence of the corrector [12]. While a constant magnitude of σ can be used throughout the continuation process, more elaborate methods of choosing the step size are described in [11, 12].

B. Parameterization and the corrective stage

The calculated values from the predictive stage need to be corrected. The corrective action is to transfer the values on to the path being traced. The variable vector for this stage can be presented as;

$$\bar{A} = [\bar{X} \quad \bar{Y} \quad \lambda]^T \quad (12)$$

Where, $\bar{A}$ is a $(2n+10m+1)\times 1$ vector. The solutions for the corrective stage can be deducted from ascertaining one variable from vector $\bar{A}$. For example $A_k = \eta$ where η is an appropriate value for the k^{th} element of $\bar{A}$, and then solving the following equations using Newton–Raphson method.

$$\begin{bmatrix} \bar{F}(\bar{A}) \\ \bar{G}(\bar{A}) \\ A_k - \eta \end{bmatrix} = \bar{0} \quad (13)$$

At each stage of the corrector in the LPC technique, only one variable of $\bar{A}$ can be certain, which is defined as the continuation parameter. This parameter corresponds to the maximum possible value in vector $\bar{t}$ [13]. Therefore, the continuation parameter will be the same variable as in the predicting stage and can be determined by:

$$\eta = \{A_k : |t_k| = MAX, \quad 2 \le k \le (10m+2n+1)\} \quad (14)$$

The continuation parameter η in the initial step is equal to λ. By approaching the voltage stability margin ($d\lambda = 0$), λ reaches its critical value ($\lambda^{critical}$). Beyond the critical point, λ tends to decrease and variations of λ become negative. Therefore, $d\lambda$ can be taken as an index to discriminate the voltage stability margin, and consequently, for voltage stability analysis, when high accurate response is vital, using this technique stands out as a solution.

IV. NUMERICAL RESULTS

The proposed scheme for the voltage stability monitoring has been applied to the New England 39-bus test system. The system consists of 18 load busses, 10 generators, and 46 lines. The system generators are located at busses 30, 31, 32, 33, 34, 35, 36, 37, 38, and 39. The data related to this system is given in [7]. In this section, the system demand is increased from its initial value to the voltage collapse point. The load ramp applied to each bus is proportional to their original demand, and only the PQ constant load model has been used to represent the demand busses. Similarly, the generation ramp applied to each generator is proportional to its original generation dispatch.

At first, the AVR voltage limits have been removed to study the effects of considering the DAEs of power system components. To elaborate the difference between the available MW margin to the point of voltage instability obtained by the CPF method and the proposed method, the P-V curve for load bus 8 are shown in Fig. 1.

As it is shown, the available MW margin obtained by the proposed method is less than the available MW margin obtained by the CPF method. It is concluded that, the power flow assumptions cause the available MW margin to be 1000 MW greater than the real value. As a result a detailed dynamic representation of the power system is required to analyze the system's stability behavior.

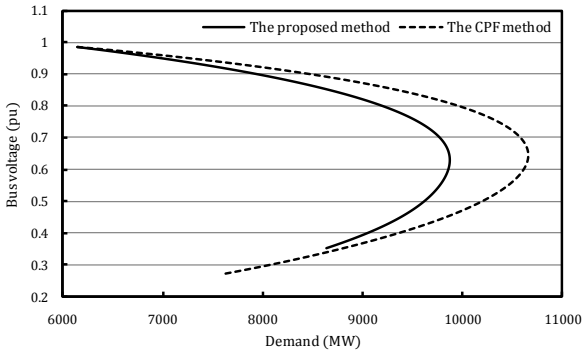

Fig. 1. The voltage of bus of 8.

Figs. 2 and 3 represent the AVR voltage and the reactive generation power, respectively, in busses 31 and 38 obtained through the proposed method during demand increase from the initial equilibrium point to the voltage collapse point. As Fig. 2 shows, the AVR voltage of busses 31 and 38 monotonously grow from the initial values of 2.59 and 2.12 p.u. to the final values at the voltage collapse of 5.99 and 4.41 p.u., respectively. Accordingly, the demand evolves from an initial value of 6141 MW to a final value at the voltage collapse of 9868 MW. Similarly, As Fig. 3 illustrates, the reactive generation power of busses 31 and 38 monotonously grow from the initial values of 275 and 140 MVAR to the final values at the voltage collapse of 1350 and 906 MVAR, respectively.

As will be seen, if the maximum AVR voltage limit of the generation units is considered,

the saturation of the AVR voltage limits of a unit may result in a deterioration of the voltage stability. Expectedly, in highly loaded cases, sometimes saturation of the AVR voltage limits of a unit can change the system voltages immediately from a stable to an unstable state. Thus, a dynamic voltage collapse leading to blackout follows.

Technical data of the AVR upper limit of the generation units of 31 and 38 used in the current study, are presented in Table I, and in the next simulations, the AVR upper limits of generators are modeled.

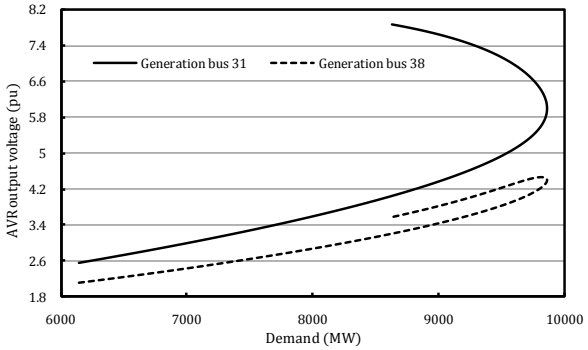

Fig. 2. The AVR voltage of busses of 31 and 38.

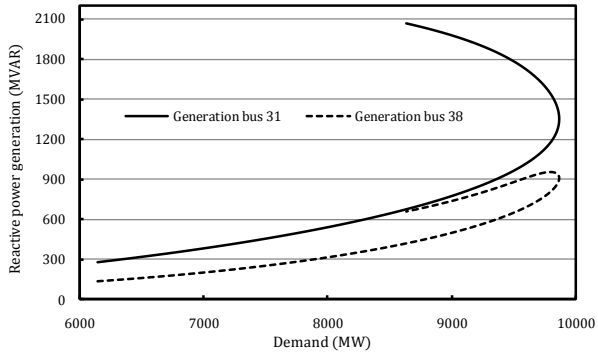

Fig. 3. The reactive generation power of busses of 31 and 38.

Table I. The AVR upper limit of the generation units of 31 and 38

Generation bus number	The AVR voltage limits (p.u.)
	Maximum
31	3.81
38	3.44

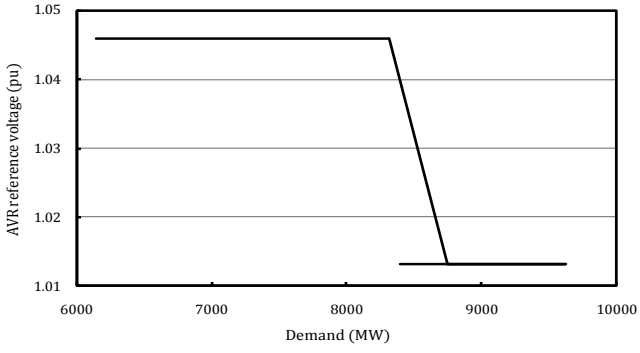

Fig. 4. The AVR reference voltage of bus of 31.

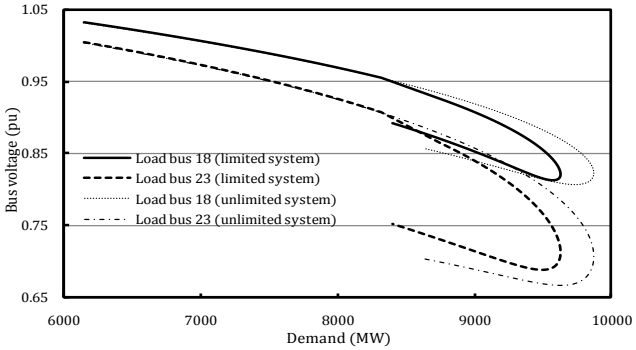

Fig. 5. The voltage of busses of 18 and 23.

The first scenario considers the AVR voltage limit of bus of 31. The AVR voltage of bus of 31 reaches their limit at value of demand of 8317 MW. Fig. 4 represents the AVR reference voltage variations. This is while the demand increases until it reaches to the voltage collapse point. As Fig. 4 shows, the AVR reference voltage evolution of bus of 31 will be constant until 8317 MW. Beyond this point, the voltage decreases, because the AVR reference voltage is considered as another state variable which changes according to the system demand. To illustrate the available MW margin to the point of voltage instability, as the demand grows, the evolution of the voltages of the load busses 18 and 23 have been depicted in Fig. 5. As it is clear, saturation of the AVR voltage limit of unit of 31 decreases the load bus voltages gradient with respect to the system demand. Thus, the AVR saturation results in deterioration of voltage stability. Because the voltages of the load busses remain in the stable region of the nose curves, the system stability is maintained and therefore, the point of voltage instability is equivalent to the SNB.

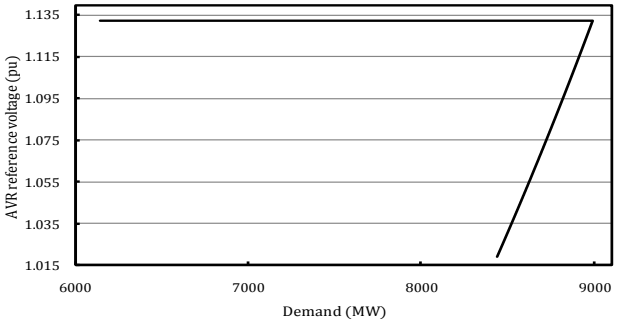

Fig. 6. The AVR reference voltage of bus of 38.

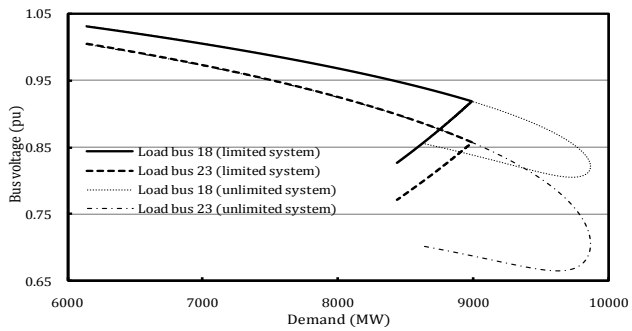

Fig. 7. The voltage of busses of 18 and 23.

The second scenario considers the AVR voltage limit of bus of 38. The AVR voltage of bus of 38 reaches their limit at value of demand of 9000 MW.

Fig. 6 represents the AVR reference voltage variations. This is while the demand increases until it reaches to the voltage collapse point. As Fig. 6 shows, the AVR reference voltage evolution of bus of 38 will be constant until 9000 MW. Beyond this point, the voltage decreases, because the AVR reference voltage is considered as another state variable which changes according to the system demand.

To illustrate the available MW margin to the point of voltage instability, as the demand grows, the evolution of the voltages of the load busses 18 and 23 have been depicted in Fig. 7. As it is clear, when the demand reaches to 9000 MW, the AVR voltage limit of unit of 38 saturates. Therefore, the sign of the load bus voltage gradient changes with respect to the system demand. Thus, the voltages of the load busses are in the unstable region of the nose curves and hence, an immediate voltage collapse will occur. The cause of this is saturation of the AVR voltage limit and therefore, the point of voltage instability is equivalent to the SLIB.

However, all of the points beyond the voltage collapse point belong to the unstable branch of the nose curves. Some unstable points have been included below stable manifold due to their importance from a topological point of view. It is important to remark that the curves are only mathematically possible, but in real power systems from an operational point of view they are unrealistic.

Consequently, for voltage stability analysis, when high accurate response is vital, using the proposed methodology stands out as a solution.

V. CONCLUSION

In this paper, a steady state voltage stability assessment of power systems was investigated by using a continuation based method. A detailed model of power system components was considered due to the accurate representation of the voltage instability phenomena. In addition, the effects of AVR voltage limits in voltage stability that indirectly control the reactive power generation were studied. This limit implementation causes either stability deterioration or immediate voltage collapse when the unlimited system evolves to a limited one.

The performance of the proposed method in the voltage stability analysis of the New England 39-bus power system model when the AVR voltage limit of one unit considered, was presented. The proposed method has the advantage of accuracy, and readily provides sensitivity information and degree of stability.

This study may be useful for two main applications:

- By means of the steady state stability margin values of busses, we can obtain an insight about the voltage security status of the power system. The larger the stability margin values of busses, the more robust the power system.
- The steady-state stability margin values may be used to determine the vulnerability of various busses in the current operating point, i.e. the low stability margin values means more vulnerability in terms of voltage security. Moreover, the most vulnerable bus with the minimum stability margin determines the stability margin of the power system.

ACKNOWLEDGMENT

The author is thankful to authorities of East Tehran Branch, Islamic Azad University, Tehran, Iran, for providing support and necessary facilities.

REFERENCES

1. G. M. Huang, N. C. Nair, “Voltage stability constrained load curtailment procedure to evaluate power system reliability measures,” In: Proceedings of IEEE/PES Winter Meeting, New York, 2002.
2. A. Tiranuchit, R. J. Thomas, “A posturing strategy against voltage instability in electric power systems,” IEEE Trans. Power Syst., vol. 3, 1998, pp. 87–93.
3. P. Kessel, H. Glavitch, “Estimating the voltage stability of a power system,” IEEE Trans. Power Deliver., vol. 1, 1986, pp. 346–354.
4. N. Amjady, “Dynamic voltage security assessment by a neural network based method,” Electr. Power Syst. Res., vol. 66, 2003, pp. 215–226.
5. F.M. Echavarren, E. Lobato, L. Rouco, “Steady-state analysis of the effect of reactive generation limits in voltage stability,” Electric Power Systems Research, vol. 79, 2009, pp. 1292–1299.
6. Y. Kataoka, Y. Shinoda, “Voltage stability limit of electric power systems with generator reactive power constraints considered,” IEEE Trans. Power Syst., vol. 20, 2005, pp. 951–962.
7. V. Ajjarapu, Computational techniques for voltage stability assessment and control, Springer, 2007.
8. P. Kundur, Power system stability and control, McGraw-Hill, 1994.
9. A. C. Z. De Souza, C. A. Canizares, V. H. Quintana, “New techniques to speed up voltage collapse computations using tangent vectors,” IEEE Trans. Power Syst., vol. 12, 1997, pp. 1380–1387.
10. A. A. Gharaveisi, M. Rashidinejad, A. Mousavi, “Voltage security evaluation based on perturbation method,” Electr. Power Energy Syst., vol. 31, 2009, pp. 227–235.
11. W. C. Rheinbolds, Numerical analysis of parameterized nonlinear equations, New York: John Wiley & Sons Interscience, 1986.
12. W. C. Rheinbolds, J. V. Burkradt, “A locally parameterized continuation process,” ACM Trans. Math. Software, vol. 9, 1983, pp. 215–235.
13. R. Seydel, From equilibrium to chaos, Elsevier, New York, 1988.

AUTHORS PROFILE

Dr. Hadi Razmi was born in Tehran, Iran, in 1980. He received the Ph.D. degree in control engineering from the Science and Research Branch, Islamic Azad University, Tehran, Iran, in 2012. He is currently an Assistant Professor of Control Engineering at East Tehran Branch, Islamic Azad University, Tehran, Iran. His research interests include power system optimization and control, security analysis, and neural networks and fuzzy systems applications.